Strain-induced polarization in wurtzite III-nitride semipolar layers

A. E. Romanov,[a] T. J. Baker, S. Nakamura, and J. S. Speck[b]
Materials Department, University of California, Santa Barbara, California 93106

(ERATO/JST UCSB Group)
University of California, Santa Barbara, California 93106

(Received 20 October 2005; accepted 6 May 2006; published online 25 July 2006)

This paper presents growth orientation dependence of the piezoelectric polarization of $In_xGa_{1-x}N$ and $Al_yGa_{1-y}N$ layers lattice matched to GaN. This topic has become relevant with the advent of growing nitride based devices on semipolar planes [A. Chakraborty *et al.*, Jpn. J. Appl. Phys., Part 2 **44**, L945 (2005)]. The calculations demonstrate that for strained $In_xGa_{1-x}N$ and $Al_yGa_{1-y}N$ layers lattice matched to GaN, the piezoelectric polarization becomes zero for nonpolar orientations and also at another point ≈45° tilted from the *c* plane. The zero crossover has only a very small dependence on the In or Al content of the ternary alloy layer. With the addition of spontaneous polarization, the angle at which the total polarization equals zero increases slightly for $In_xGa_{1-x}N$, but the exact value depends on the In content. For $Al_yGa_{1-y}N$ mismatched layers the effect of spontaneous polarization becomes important by increasing the crossover point to ~70° from *c*-axis oriented films. These calculations were performed using the most recent and convincing values for the piezoelectric and elasticity constants, and applying Vegard's law to estimate the constants in the ternary $In_xGa_{1-x}N$ and $Al_yGa_{1-y}N$ layers. © *2006 American Institute of Physics*.
[DOI: 10.1063/1.2218385]

I. INTRODUCTION

Gallium nitride and its alloys with In and Al are used to produce visible and ultraviolet optoelectronic devices and high power electronic devices.[1,2] An important physical property of nitride semiconductors with the wurtzite crystal structure is their spontaneous electrical polarization.[3] Another type of electrical polarization observed for III-nitrides is strain-induced polarization, which is caused by piezoelectric properties of this group of materials.[4] The net polarization and consequent internal electric fields have been shown to be detrimental to the performance of optoelectronic devices.[5–9] Polarization discontinuities lead to band bending and result in the quantum confined Stark effect in (0001) oriented III-nitride quantum well (QW) structures. The consequences of this effect include decreased recombination efficiency, redshifted emission, and blueshifting of the emission with increasing drive current. It is well established that the total electric polarization response of crystalline solids is related to the symmetry of the crystal.[10] For the III-nitrides, the polarization response can be measured by various experimental techniques[11,12] or calculated from first principles.[3,4,13,14]

Spontaneous polarization for the III-nitrides is directed along the polar *c* axis of the hexagonal structure, which is also the common growth orientation on substrates such as (0001) saphire or (0001) SiC [see Fig. 1(a)]. To eliminate the effect of the fixed interfacial or surface polarization charges, nonpolar growth orientations can be used[15,16] as shown in Fig. 1(b). Otherwise intermediate semipolar growth orientations may be introduced [see Fig. 1(c)], which will, in part, reduce the magnitude of spontaneous polarization induced charges. Experimental work at UCSB has demonstrated the feasibility of growing planar templates of GaN in semipolar orientations.[17] In semipolar growth, any plane (*hkil*) with a nonzero *h*, *k*, or *i and* a nonzero *l* Miller index can, in principle, serve as a growth surface. However, only low index semipolar planes can be used to realize reliably smooth templates. GaN $\{10\bar{1}1\}$, $\{10\bar{1}3\}$, and $\{11\bar{2}2\}$ templates have been grown by hydride vapor phase epitaxy (HVPE) and by metal organic chemical vapor deposition (MOCVD); only one example of a semipolar plane is shown in Fig. 1(c) for clarity. Semipolar templates have already been used for successful fabrication of light emitting diodes (LEDs).[18]

Strain-induced polarization depends on the nature of pi-

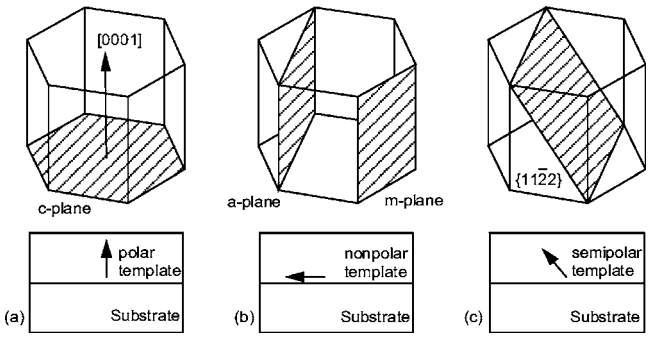

FIG. 1. Crystallography and *c*-axis orientation for the growth of III-nitride layers: (a) Polar growth with the *c* axis normal to the layer surface; the growth plane is the (0001) *c* plane, (b) Nonpolar growth with *c* axis parallel to the layer surface; possible growth planes include the $\{11\bar{2}0\}$ *a* plane and the $\{1\bar{1}00\}$ *m* plane, (c) Semipolar growth with the *c* axis inclined with respect to the layer surface. This example shows the $\{11\bar{2}2\}$ growth plane.

[a]Permanent address: Ioffe Physico-Technical Institute, Russian Academy of Sciences, St. Petersburg 194021, Russia.
[b]Electronic mail: speck@mrl.ucsb.edu

ezoelectric coupling and the strain state. For the III-nitride layers, (e.g., QW structures widely used in modern optoelectronic devices) grown on commonly oriented templates with *c* plane as a growth plane, strains arise because of the equibiaxial crystal lattice mismatch between the layer and template materials. For such polar growth, the effects of polarization are very pronounced and important, e.g., Refs. 7 and 19. If grown on nonpolar or semipolar templates [shown in Figs. 1(b) and 1(c)], the layer/template mismatch can vary considerably from the equibiaxial case, which will also change the piezoelectric polarization.

In QW structures, a thin layer of chemically different or modified material grown pseudomorphically on a template becomes elastically strained to match the template crystal lattice. The layer then can be covered by matrix template material to form a buried QW. Both the surface and buried layers remain elastically strained (without any plastic relaxation) if their thickness is below a critical thickness for misfit dislocation formation.[20] Even the layers grown beyond the critical thickness usually demonstrate incomplete plastic relaxation (which is well documented for III-nitride mismatched layers, e.g., see Refs. 21 and 22) that leads to strain-induced electrical polarization.

A number of attempts have focused on the electrical polarization and polarization-related effects in strained III-nitride semipolar layers with arbitrary orientation of the *c* axis with respect to the layer surface (or interfaces), e.g., see Refs. 23–26. These studies are based on approaches developed previously for calculation of strain-induced effects in cubic semiconductor QW structures.[27–29] Despite the interesting physical predictions (e.g., the existence of specific template orientations with no polarization discontinuity between the strained layer and template), the results of the early studies cannot be applied for the rigorous modeling of real semipolar III-nitride layers because of shortcomings in assumptions for either the mechanics of the strained layers or the piezoelectric response of the material.

The aim of the present article is to provide a comprehensive analysis of electrical polarization in strained III-nitride layers (ternary $In_xGa_{1-x}N$ and $Al_yGa_{1-y}N$ alloys) pseudomorphically grown on wurtzite GaN templates of arbitrary semipolar orientation. Our approach is motivated by recent growth experiments on semipolar nitride layers[17] and is based on correct elasticity calculations, which include proper boundary conditions and complete wurtzite elastic anisotropy. The model accounts for the dependence of crystal lattice mismatch between the layer and the template on the growth plane orientation. The model also includes the dependence of c/a aspect ratio on the composition of ternary $In_xGa_{1-x}N$ and $Al_yGa_{1-y}N$ alloys, which is also the basis for the dependence of the crystal lattice mismatch on the growth template crystallographic orientation. For numerical calculations of piezoelectric and total polarizations the most updated values of elastic and piezoelectric coefficients were used in combination with Vegard's law for all parameters for ternary alloys.

The results demonstrate that for an $In_xGa_{1-x}N$ (or $Al_yGa_{1-y}N$) quantum well with GaN barriers, the piezoelectric polarization becomes zero for nonpolar orientations and also at another orientation ~45° tilted from the *c* plane. There exists also an extremum of the polarization between 45° and 90° *c*-axis inclination. The zero polarization crossover has only a very small dependence on the In or Al percentage of the ternary alloy layer. With the addition of spontaneous polarization, there is a change of the orientation angle at which the interface difference of total polarization equals zero. This change is rather small for $In_xGa_{1-x}N$ layers, but is significant for $Al_yGa_{1-y}N$ layers.

II. EXPERIMENTAL MOTIVATION

Recent growth studies have revealed that several semipolar orientations can be grown epitaxially on spinel and sapphire substrates.[17,30] The semipolar epitaxial relationships discovered on these substrates were $(10\bar{1}\bar{1})$ GaN on {100} spinel, $(10\bar{1}\bar{3})$ GaN on {110} spinel, and both $(10\bar{1}\bar{3})$ and $(11\bar{2}2)$ GaN on $\{10\bar{1}0\}$ sapphire. Figure 2 illustrates these semipolar GaN orientations with their principal crystallographic directions on the respective substrates.

The structural properties of the samples grown in semipolar orientation were found to be similar to those for the samples grown in nonpolar orientations. The threading dislocation density was on the order of 10^9-10^{10} cm^{-2} on average. The threading dislocations had line directions that were in the $\langle 10\bar{1}0\rangle$ directions for all the films. Therefore those dislocations were inclined with respect to the surface. The stacking fault density was approximately 2×10^5 cm^{-1} for all the films. The rms roughness as measured by atomic force microscopy ranged from 4 to 8 nm for an area of 25 μm^2. For the $(10\bar{1}\bar{1})$ and $(10\bar{1}\bar{3})$ films, the $[000\bar{1}]$ direction was directed toward the film surface normal, thus these layers had N-face sense polarity. The $(11\bar{2}2)$ films had the positive [0001] direction in the outward sense and thus the film had Ga-face sense polarity.

The growth orientation on *m*-plane sapphire can be selected by the early stage HVPE growth conditions. A low temperature nitridation step produced by ramping in ammonia will give $(11\bar{2}2)$ GaN. A high temperature nitridation step will result in $(10\bar{1}\bar{3})$ GaN. For the high temperature nitridation, the substrate was ramped in nitrogen and hydrogen until the temperature reached 1000 °C, then ammonia was flowed for 10 min before the growth was initiated. X-ray diffraction has shown that this procedure achieved phase purity in the films.

The crystallography of the semipolar films, which have been experimentally realized, is either $(10\bar{1}n)$ or $(11\bar{2}n)$. For $(10\bar{1}n)$ case the tilt is about one of $\langle 11\bar{2}0\rangle$ directions in GaN, whereas for $(11\bar{2}n)$ case, the tilt is about one of $\langle 10\bar{1}0\rangle$ directions. The sixfold symmetry of the wurtzite crystal structure on the basal plane dictates its isotropy [the piezoelectric and elastic properties are the same for any direction within the (0001) plane[10]]. Hence, for purposes of our investigation, only the consideration of the angle between the semipolar plane and basal plane is important.

To characterize each semipolar plane, we used basic crystallography to calculate the angle between the semipolar

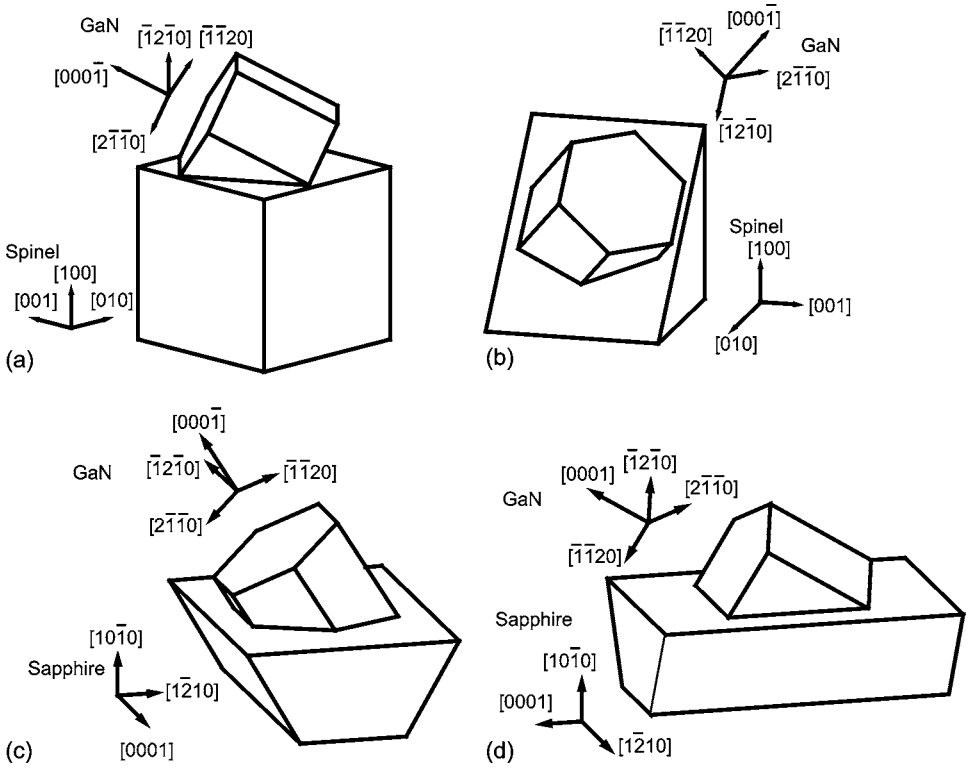

FIG. 2. Crystallography of grown semipolar structures: (a) $(10\bar{1}\bar{1})$ GaN on {100} spinel, (b) $(10\bar{1}\bar{3})$ GaN on {100} spinel, (c) $(10\bar{1}3)$ GaN on $\{10\bar{1}0\}$ sapphire, and (d) $(11\bar{2}\bar{2})$ GaN on $\{10\bar{1}0\}$ sapphire.

plane and the basal plane. The $(10\bar{1}\bar{3})$ plane intersects the c plane at 32.0°, the $(10\bar{1}\bar{1})$ plane at 62.0°, and the $(11\bar{2}2)$ plane at 58.4° for GaN. However, the c/a ratio is different for AlN, InN, and GaN, so the angles between planes are not exactly the same for different compositions, as shown in Table I. The largest difference in c/a ratios is for AlN and GaN. In this case, the [0001] directions will be different by ~0.4° when AlN and GaN are lattice matched on a semipolar plane. A typical $In_{1-x}Ga_xN$ QW on GaN will only have the [0001] directions diverging by ~0.1°. Therefore we neglect this effect and only consider the inclination angles as for GaN template.

III. MECHANICS AND PIEZOELECTRIC RESPONSE OF STRAINED NITRIDE LAYERS

A. The model

We consider here $In_xGa_{1-x}N$ and $Al_yGa_{1-y}N$ QW structures grown pseudomorphically on GaN templates. These structures may include multiple or single buried QW or a single layer on GaN template as shown in Fig. 3. In the following we use the notation "layer" for the material with modified chemical composition both for buried QW or free surface film. For crystal lattice parameters a_L and c_L of wurtzite layers we apply Vegard's law:

$$a_L = x \cdot a_{\mathrm{InN}} + (1-x) \cdot a_{\mathrm{GaN}}, \quad c_L = x \cdot c_{\mathrm{InN}} + (1-x) \cdot c_{\mathrm{GaN}}, \tag{1}$$

$$a_L = y \cdot a_{\mathrm{AlN}} + (1-y) \cdot a_{\mathrm{GaN}}, \quad c_L = y \cdot c_{\mathrm{AlN}} + (1-y) \cdot c_{\mathrm{GaN}}, \tag{2}$$

for $In_xGa_{1-x}N$ or $Al_yGa_{1-y}N$ layers, respectively. The crystal lattice parameters of the template are those of GaN:

$$a_T = a_{\mathrm{GaN}}, \quad c_T = c_{\mathrm{GaN}}. \tag{3}$$

It is assumed that the c axis in GaN template is inclined at the angle ϑ with respect to the normal vector of the template's surface. To describe the strain state and polarization in the layer, we use two coordinate systems xyz and $x'y'z'$ [see Fig. 3(a)] correspondingly designated as the N- and P-coordinate systems (for the "natural" and "primed" coordinate systems), respectively. The natural coordinate z is in the direction [0001] of the wurtzite crystal lattice, two other natural coordinates x and y are in the basal (0001) plane. Because of the property of isotropy of the basal plane, the mutually perpendicular directions in the basal plane can be aligned along two arbitrarily perpendicular directions of the $\langle uv\bar{u}+\bar{v}0\rangle$ type. For definitiveness and simplicity, we choose the x axis along $[11\bar{2}0]$ and the y axis along $[\bar{1}100]$. In the primed P-coordinate system the z' axis is in the direction of the template's surface normal, the two other axes (x' and y')

TABLE I. Lattice parameters and inclination angles for crystallographic planes of III-nitrides with wurtzite structure. The angles given are the angles between the semipolar plane and the c plane for each experimentally realized semipolar plane. The different c/a ratios for InN, GaN, and AlN dictate that the angles of these low symmetry planes are not the same for all III-nitrides. Data for lattice parameters a and c are taken from Ref. 31.

	AlN	GaN	InN
a (Å)	3.112	3.189	3.54
c (Å)	4.982	5.185	5.705
c/a	1.601	1.626	1.612
$(10\bar{1}\bar{3})$	31.64°	32.04°	31.81°
$(11\bar{2}\bar{2})$	58.01°	58.41°	58.18°
$(10\bar{1}\bar{1})$	61.59°	61.96°	61.75°

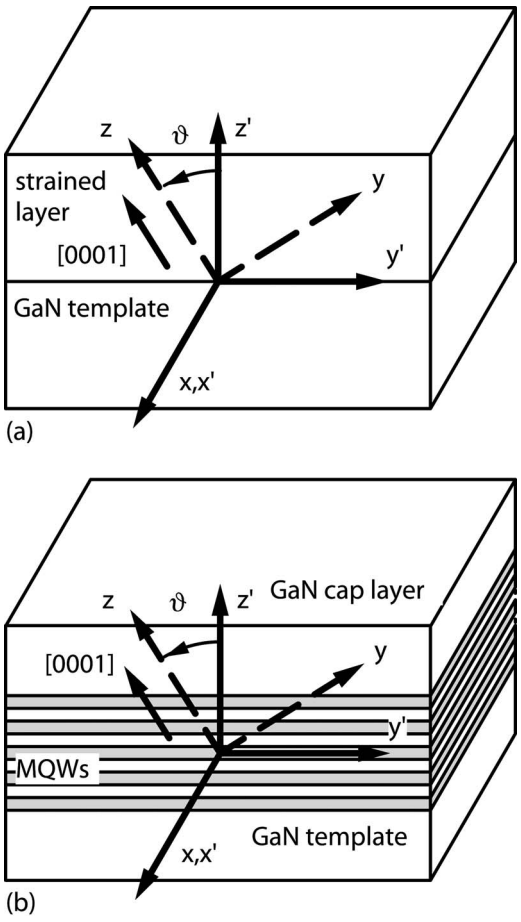

FIG. 3. Coordinate systems used in calculations of strain induced polarization: *xyz*—natural coordinate system associated with *c* axis; $x'y'z'$—coordinate system related to the layer surface normal. (a) Single mismatched layer and (b) multiple buried layers (quantum wells).

are in the template's surface plane with the x' axis coincident with the x axis—this axis also serves as the rotation axis for the *c*-axis inclination.

As a result of pseudomorphic growth, a thin layer is constrained by the template in such a way that it mimics the orientation of crystallography directions and planes of the thick template. This means that the interface between the layer and template has to obey the same crystallography for both contacting phases. This property will allow us to define misfit parameters that control elastic strain in the layer. To calculate misfit parameters ε_{m1} and ε_{m2} along two mutually perpendicular directions (i.e., along the x' and y' axes) at the interface, we consider the schematic shown in Fig. 4, in which the part of the material bounded by low index crystallography planes of the wurtzite structure is shown. The plane *BCD* is the interface between layer and template and it is perpendicular to the plane *ABO*. The normal to the plane *BCD* coincides with the z' direction, and the *c* axis (which is parallel to the z direction) is inclined by an angle ϑ. Using this configuration the following relations can be easily derived:

$$CD_T = a_T,\ \ OA_T = \sqrt{3}a_T,\ \ AB_T = \sqrt{3}a_T \tan\vartheta,\ \ OB_T = \frac{\sqrt{3}a_T}{\cos\vartheta}. \tag{4}$$

Then we have to find the crystallographically equivalent distances for the layer material. The key issue is the assumption that AB_L in an unconstrained state scales from AB_T proportional to the $\frac{c_L}{c_T}$ ratio:

$$AB_L = \frac{c_L}{c_T} AB_T. \tag{5}$$

From Eq. (5) and simple geometrical considerations, it follows that

$$\begin{aligned} &CD_L = a_L, \quad OA_L = \sqrt{3}a_L, \quad AB_L = \frac{c_L}{c_T}\sqrt{3}a_T \tan\vartheta, \\ &OB_L = \sqrt{OA_L^2 + AB_L^2} \\ &\quad = \frac{\sqrt{3}}{c_T \cos\vartheta}\sqrt{(a_L c_T)^2 \cos^2\vartheta + (a_T c_L)^2 \sin^2\vartheta}. \end{aligned} \tag{6}$$

Finally, two misfit parameters are defined as follows:

$$\begin{aligned} &\varepsilon_{m1} \equiv \frac{CD_T - CD_L}{CD_L} = \frac{a_T - a_L}{a_L}, \\ &\varepsilon_{m2} \equiv \frac{OB_T - OB_L}{OB_L} \\ &\quad = \frac{a_T c_T - \sqrt{(a_L c_T)^2 \cos^2\vartheta + (a_T c_L)^2 \sin^2\vartheta}}{\sqrt{(a_L c_T)^2 \cos^2\vartheta + (a_T c_L)^2 \sin^2\vartheta}}. \end{aligned} \tag{7}$$

It is remarkable that the misfit parameters defined by Eqs. (7) do not depend on the direction of the misorientation axis—there are no other parameters involved except the crystal lattice constants and inclination angle ϑ. The other important property of the misfit parameters can be determined under the condition of unchanged aspect ratio $\frac{c_T}{a_T} = \frac{c_L}{a_L} = \text{const}$ between crystal lattice cells in the template and in the layer. In this case $\varepsilon_{m2} = \varepsilon_{m1}$, and there is no dependence of the mismatch on the inclination angle ϑ.

For the two limiting cases $\vartheta = 0$ and $\vartheta = 90°$ the second formula from Eqs. (7) provides an obvious result:

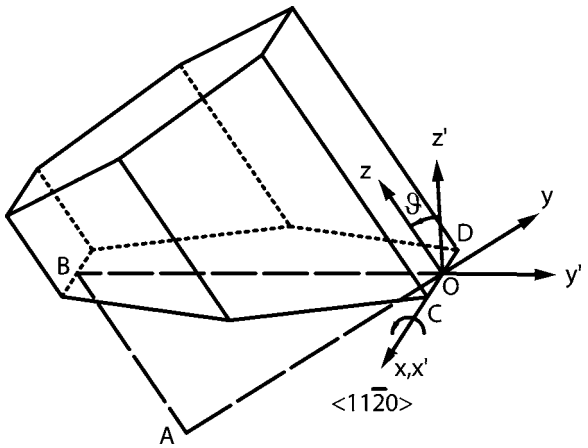

FIG. 4. Schematic for the determination of crystal lattice mismatch between a semipolar oriented layer and the template. Inclination axis is along $\langle 11\bar{2}0\rangle$ type direction in the basal plane.

$$\varepsilon_{m2}|_{\vartheta=0} = \frac{a_T - a_L}{a_L}, \quad \varepsilon_{m2}|_{\vartheta=90^\circ} = \frac{c_T - c_L}{c_L}. \tag{8}$$

This means that for (0001) oriented layers the mismatch is equibiaxial, but for nonpolar layers, in the general case for changing aspect ratio with chemical composition of the layer, there is a deviation from the equibiaxial mismatch. Finally, semipolar layers will demonstrate the dependence of mismatch (for one of the misfit parameters) on the growth plane orientation.

B. Elastic strains in anisotropic mismatched III-nitride layers

The crystal lattice mismatch (which can be quantitatively described by the misfit parameters ε_{m1} and ε_{m2}) is the reason for elastic strain and mechanical stress in coherently (pseudomorphically) grown layers on thick substrates (templates). In the case that the layer thickness is below a critical thickness for misfit dislocation formation[20] and the template can be considered as infinitely thick, all mismatch are accommodated by the elastic strain of the layer. In the *P*-coordinate system related to the layer normal, three components of the elastic strain can be directly found from the constrained conditions at the layer/template interface:

$$\varepsilon_{x'x'} = \varepsilon_{m1}, \quad \varepsilon_{y'y'} = \varepsilon_{m2}, \quad \varepsilon_{x'y'} = 0. \tag{9}$$

The last relation in Eqs. (9) implies the absence of in-plane shear mismatch at the interface between the layer and the template. It follows directly from the schematics in Fig. 4 that such shear mismatch vanishes for the geometry of semipolar wurtzite-type templates under consideration. The other set of relations follow from the conditions of mechanical equilibrium in the layer/template system:

$$\sigma_{z'z'} = 0, \quad \sigma_{x'z'} = 0, \quad \sigma_{y'z'} = 0, \tag{10}$$

where $\sigma_{k'm'}$ are stress tensor components in the *P*-coordinate system. These conditions simply indicate that the free surface is traction-free. For buried layers, which are covered by template material [as shown in Fig. 4(b)], the same conditions hold. In addition to six equations given in Eqs. (9) and (10), six other relations follow from the Hook's law:

$$\sigma_{k'm'} = C_{k'm'i'j'}\varepsilon_{i'j'}, \tag{11}$$

where $C_{k'm'i'j'}$ are the components of the fourth-rank elastic stiffness tensor given in the *P*-coordinate system. Usually, the elastic stiffness are given in compact 6×6 matrix Voigt notation C_{km}.[10] For materials with the wurtzite structure, the standard form of the C_{km} matrix is based on the *N*-coordinate system with the z axis labeled by the index "3" and has five independent matrix elements, i.e., C_{11}, C_{12}, C_{13}, C_{33}, and C_{44}.

All together relations (9)–(11) provide a well defined system of 12 equations, which can be solved for the 12 components of elastic strains and stresses in mismatched layers. The details of the solution are given in the Appendix. In the *P*-coordinate system the nonzero components of strain tensor are

$$\begin{aligned}
&\varepsilon_{x'x'} = \varepsilon_{m1},\\
&\varepsilon_{y'y'} = \varepsilon_{m2},\\
&\varepsilon_{z'z'} = \frac{(B_{41}\varepsilon_{m1} + B_{42}\varepsilon_{m2})A_{32} - (B_{31}\varepsilon_{m1} + B_{32}\varepsilon_{m2})A_{42}}{A_{31}A_{42} - A_{32}A_{41}},\\
&\varepsilon_{y'z'}\frac{(B_{31}\varepsilon_{m1} + B_{32}\varepsilon_{m2})A_{41} - (B_{41}\varepsilon_{m1} + B_{42}\varepsilon_{m2})A_{31}}{A_{31}A_{42} - A_{32}A_{41}},
\end{aligned} \tag{12}$$

where

$$A_{31} = C_{11}\sin^4\vartheta + \left(\frac{1}{2}C_{13} + C_{44}\right)\sin^2 2\vartheta + C_{33}\cos^4\vartheta,$$

$$A_{32} = [C_{11}\sin^2\vartheta + (C_{13} + 2C_{44})\cos 2\vartheta - C_{33}\cos^2\vartheta]\sin 2\vartheta,$$

$$A_{41} = \frac{1}{2}[(C_{11} - C_{13})\sin^2\vartheta + 2C_{44}\cos 2\vartheta + (C_{13} - C_{33})\cos^2\vartheta]\sin 2\vartheta,$$

$$A_{42} = \left(\frac{C_{11} + C_{33}}{2} - C_{13}\right)\sin^2 2\vartheta + 2C_{44}\cos^2 2\vartheta,$$

$$B_{31} = C_{12}\sin^2\vartheta + C_{13}\cos^2\vartheta,$$

$$B_{32} = C_{13}(\sin^4\vartheta + \cos^4\vartheta) + \left(\frac{C_{11} + C_{33}}{4} - C_{44}\right)\sin^2 2\vartheta,$$

$$B_{41} = \frac{C_{12} - C_{13}}{2}\sin 2\vartheta,$$

$$B_{42} = \frac{1}{2}[C_{11}\cos^2\vartheta - (C_{13} + 2C_{44})\cos 2\vartheta - C_{33}\sin^2\vartheta]\sin 2\vartheta,$$

with ε_{m1} and ε_{m2} given by Eq. (7) and the elastic stiffness coefficients of the layer material.

In the *N*-coordinate system nonzero strains can be determined from the values given by Eq. (12) by applying the appropriate tensor transformation as follows:

$$\begin{aligned}
&\varepsilon_{xx} = \varepsilon_{x'x'},\\
&\varepsilon_{yy} = \varepsilon_{y'y'}\cos^2\vartheta + \varepsilon_{z'z'}\sin^2\vartheta + \varepsilon_{y'z'}\sin 2\vartheta,\\
&\varepsilon_{zz} = \varepsilon_{y'y'}\sin^2\vartheta + \varepsilon_{z'z'}\cos^2\vartheta - \varepsilon_{y'z'}\sin 2\vartheta,\\
&\varepsilon_{yz} = \frac{\varepsilon_{z'z'} - \varepsilon_{y'y'}}{2}\sin 2\vartheta + \varepsilon_{y'z'}\cos 2\vartheta.
\end{aligned} \tag{13}$$

The analysis of the strain tensor components given in Eq. (13) demonstrates that our calculations correct the approximations and mistakes of Refs. 24–26.

C. Spontaneous and strain-induced polarization

The presence of electric polarization is directly related to the crystal symmetry. Nitride semiconductors exist in both the zinc blende and wurtzite structures. In both cases, each group-III atom is tetrahedrally coordinated to four nitrogen atoms. The main difference between these two structures is the stacking sequence of close packed diatomic planes. These stacking sequences are *ABABAB* along the wurtzite [0001] direction and *ABCABC* along the zincblende {111} directions. This difference in stacking sequence results in distinct space group symmetries: $P6_3mc$ for wurtzite and $F\bar{4}3m$ for zinc blende.

In the absence of external electric fields, the total macroscopic polarization **P** of a solid is the sum of the spontaneous polarization of the equilibrium structure $\mathbf{P}^{\mathrm{sp}}$ and of the strain-induced, piezoelectric polarization $\mathbf{P}^{\mathrm{pz}}$. Nitride semiconductors with wurtzite structure demonstrate a single polar axis, namely, the [0001] axis. Thus, the wurtzite phase has a net spontaneous electrical polarization along [0001] even at equilibrium, which is different from compound semiconductors with the zinc blende structure.

As we already discussed in the previous section, semiconductor layers are often grown under strain due to the lattice mismatch to the underlying template. Such deformations of the unit cell can lead to additional piezoelectric polarization. The presence of this kind of polarization is again closely related to the unit cell symmetry, namely, the lack of inversion symmetry. Layers grown in polar orientation are under in-plane biaxial stretching or contraction and the crystal exhibits a strain-induced or piezoelectric polarization. In general, for semipolar growth the elementary cell of material under consideration can be subjected to an arbitrary strain ε_{ij}. By taking into account the symmetry of the space group $P6_3mc$ of wurtzite III-nitrides, the piezoelectric polarization is related to strains as

$$\mathbf{P}^{\mathrm{pz}} = \begin{pmatrix} 0 & 0 & 0 & 0 & e_{15} & 0 \\ 0 & 0 & 0 & e_{15} & 0 & 0 \\ e_{31} & e_{31} & e_{33} & 0 & 0 & 0 \end{pmatrix} \begin{pmatrix} \varepsilon_{xx} \\ \varepsilon_{yy} \\ \varepsilon_{zz} \\ \varepsilon_{yz} \\ \varepsilon_{xz} \\ \varepsilon_{xy} \end{pmatrix} = \begin{pmatrix} e_{15}\varepsilon_{xz} \\ e_{15}\varepsilon_{yz} \\ e_{31}(\varepsilon_{xx}+\varepsilon_{yy}) + e_{33}\varepsilon_{zz} \end{pmatrix}, \tag{14}$$

with the elements e_{ij} of the piezoelectric tensor in Voigt notation.[4,10] We note that the relations of Eq. (14) are given in the natural *N*-coordinate system relative to the *c* axis. Any spatial change in total polarization **P** leads to a fixed volume charge density:

$$\rho = -\nabla \cdot \mathbf{P}. \tag{15}$$

For steplike (abrupt) change in the polarization (for example, at the AlGaN/GaN interface) Eq. (15) should be modified to give fixed surface (sheet) charge density:

TABLE II. Elastic constants of III-nitrides with wurtzite structure (Ref. 32).

Elastic constants	AlN	GaN	InN
C_{11} (GPa)	396	367	223
C_{12} (GPa)	137	135	115
C_{13} (GPa)	108	103	92
C_{33} (GPa)	373	405	224
C_{44} (GPa)	116	95	48

$$q = -\mathbf{n} \cdot \Delta\mathbf{P}, \tag{16}$$

where **n** is the vector normal to the free surface or to the interface, and $\Delta\mathbf{P}$ is the change in total polarization. Key examples of fixed charges *q* at AlGaN/GaN interface give rise to two-dimensional electron gases and alternating sheet charge in InGaN/GaN quantum wells, which give rise to the quantum-confined Stark effect (e.g., see Ref. 19 and references therein).

In the following analysis we calculate the polarization discontinuity at the interfaces of strained III-nitride layers grown in semipolar geometry as shown in Fig. 4. The polarization component $\Delta P_{z'}$, which is responsible for the surface charge density *q*, should be determined in the *P*-coordinate system:

$$\Delta P_{z'} = P^{\mathrm{pz}}_{Lz'} + (P^{\mathrm{sp}}_{L} - P^{\mathrm{sp}}_{T})\cos\vartheta, \tag{17}$$

where P^{sp}_{L} and P^{sp}_{T} are the spontaneous polarizations for the layer and the template, respectively, with strain-induced piezoelectric polarization component $P^{\mathrm{pz}}_{Lz'}$ of the layer possessing a complex dependence on the orientation ϑ due to the tensor character of the strain transformation [and also described by Eq. (7), i.e., dependence of the misfit parameter $\varepsilon_{m2}(\vartheta)$]:

$$\begin{aligned} P^{\mathrm{pz}}_{Lz'} = {} & e_{31}\cos\vartheta\varepsilon_{x'x'} \\ & + \left(e_{31}\cos^3\vartheta + \frac{e_{33}-e_{15}}{2}\sin\vartheta\sin 2\vartheta\right)\varepsilon_{y'y'} \\ & + \left(\frac{e_{33}+e_{15}}{2}\sin\vartheta\sin 2\vartheta + e_{33}\cos^3\vartheta\right)\varepsilon_{z'z'} \\ & + [(e_{31}-e_{33})\cos\vartheta\sin 2\vartheta + e_{15}\sin\vartheta\cos 2\vartheta]\varepsilon_{y'z'}, \end{aligned} \tag{18}$$

where all strains are defined in the *P*-coordinate system by Eqs. (12). In the following, we will see how the interplay of the crystal elastic anisotropy and the anisotropy of the piezoelectric coefficients provides the existence of zero net normal polarization component at a particular template growth orientation.

IV. NUMERICAL RESULTS

A. Strain results

To calculate elastic strains in mismatched layers grown on semipolar GaN templates, we use well-established lattice parameters for III-nitrides (Table I and Ref. 31) together with elastic stiffnesses given by Wright (Table II and Ref. 32). The values for stiffness coefficients in the layer were calcu-

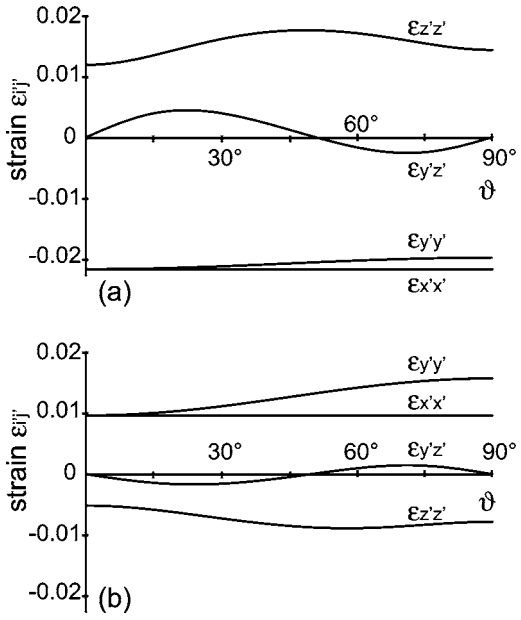

FIG. 5. Elastic strains in anisotropic mismatched layer as a function of c-axis inclination angle ϑ in P-coordinate system for mismatched (a) $In_{0.2}Ga_{0.8}N$ and (b) $Al_{0.4}Ga_{0.6}N$ layers on a semipolar GaN template.

lated using Vegard's law with the values $x=0.05$, 0.10, 0.15, and 0.20 for $In_xGa_{1-x}N$ and $y=0.10$, 0.20, 0.30, and 0.40 for $Al_yGa_{1-y}N$ compositions. Figure 5 presents the dependence of the strain components on the c-axis inclination angle ϑ in the P-coordinate system calculated with Eqs. (12). Two sets of compositions correspond to biaxial compression [Fig. 5(a)] or biaxial tension [Fig. 5(b)]. Obviously the strain component $\varepsilon_{z'z'}$ in the out-of-plane direction has the opposite sign to in-plane strains due to Poisson's effect. The strain behavior in the N-coordinate system shown in Fig. 6 is less obvious because of the changing orientation of the N-coordinate system.

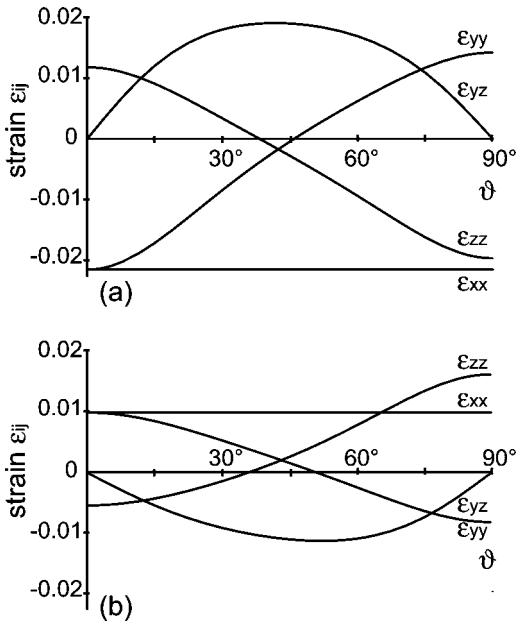

FIG. 6. Elastic strains in anisotropic mismatched layer as function of c-axis inclination angle ϑ in N-coordinate system for mismatched (a) $In_{0.2}Ga_{0.8}N$ and (b) $Al_{0.4}Ga_{0.6}N$ layers on a semipolar GaN template.

TABLE III. Piezoelectric coefficients and spontaneous polarization P_{sp} of III-nitrides with the wurtzite structure.

Piezoelectric coefficients	AlN	GaN	InN
e_{33} (cm^{-2})	1.55[a]	0.73[b]	0.73
e_{31} (cm^{-2})	−0.58[a]	−0.49[b]	−0.49
e_{15} (cm^{-2})	−0.48[a]	−0.40[b]	−0.40
P_{sp} (cm^{-2})	−0.081[c]	−0.029[c]	−0.032[c]

[a]Experimental data from Ref. 33.
[b]Used in Ref. 34.
[c]Calculated in Ref. 3.

B. Polarization results

We use values for spontaneous polarization in III-nitrides given in Table III (see Refs. 3, 33, and 34). Again for the layers with varying compositions, Vegard's law was applied. For piezoelectric coefficients e_{ij} we could not find reliable data for InN (for a detailed discussion see Ref. 19; note that, for example, in Refs. 31 and 35 the coefficient e_{15} has opposite signs!), for which we just use the data for GaN as shown in Table III. Since the value of spontaneous polarization for GaN and InN are nearly the same, we anticipate similar values of their piezoelectric coefficients. However, for $Al_yGa_{1-y}N$ compositions, we applied Vegard's law based on the piezoelectric coefficients given in Table III. We discuss the limitations in the use of Vegard's law for various model parameters below.

Figure 7 presents the results for the normal component of strain-induced polarization $P^{pz}_{Lz'}$ and total change of the polarization at the layer/template interface $\Delta P_{z'}$ for $In_xGa_{1-x}N$ layers on a GaN substrate (under compression) for $x=5\%$, 10%, 15%, and 20%. Figure 8 shows the same quantities for $Al_yGa_{1-y}N$ layers on GaN substrate (under tension) for $y=10\%$, 20%, 30%, ande 40%.

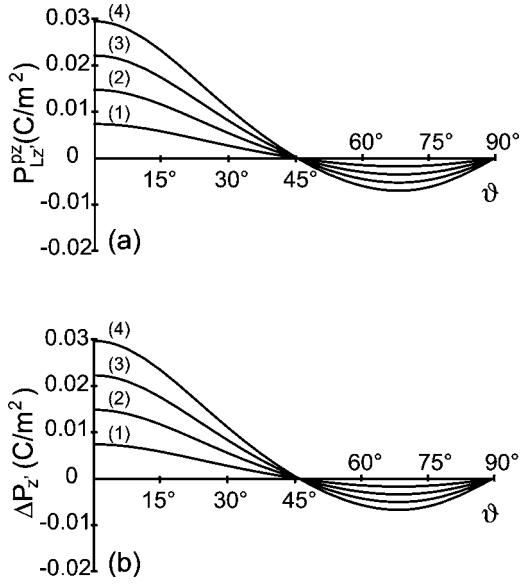

FIG. 7. Polarization effects in semipolar layers under biaxial compression. (a) Dependence of the piezoelectric polarization $P^{pz}_{Lz'}$ and (b) difference $\Delta P_{z'}$ of the total polarization on the semipolar plane orientation ϑ for In_xGa_{1-x} layers on GaN. Composition $x=0.05$ (1), 0.10 (2), 0.15 (3), and 0.20 (4).

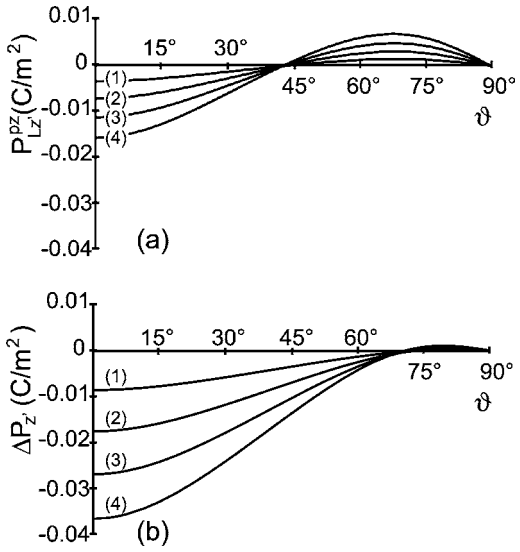

FIG. 8. Polarization effects in semipolar layers under tension. (a) Dependence of the piezoelectric polarization $P^{pz}_{Lz'}$ and (b) difference $\Delta P_{z'}$ of the total polarization on the semipolar plane orientation ϑ for $Al_yGa_{1-y}N$ layer on GaN. Composition $y=0.1$ (1), 0.2 (2), 0.3 (3), and 0.4 (4).

V. DISCUSSION AND CONCLUSIONS

The key issue in determining the piezoelectric response in mismatched III-nitride layers is the proper determination of the strain state. The strain calculations presented in this paper included the following features: (i) full set of boundary conditions for strain and stress components given by Eqs. (9) and (10); (ii) complete wurtzite-type crystal lattice elastic anisotropy given by Eq. (A4) in the matrix form for stiffness coefficients; and (iii) the dependence of the misfit parameters for the mismatch layer on the orientation of the template growth plane as given by Eqs. (7).

We note that the combination of all the above features [(i)–(iii)] was not included in the previous attempts[23–26] to investigate strain in semipolar III-nitride pseudomorphically grown layers. For example, in Refs. 23, 24, and 26 traction-free surface conditions were omitted. The solutions for infinite media, which were derived by minimization of total elastic energy, were used that resulted in different expressions for elastic strains in the layer. In Ref. 25 the strain calculations were performed under the assumption of an equibiaxial character of the mismatch in the layer; as a result, not all elastic and piezoelectric coefficients were included in the calculations. Recent work[19] has demonstrated the correct handling of elasticity calculations, but the detailed approach was given for only the polar case.

For the numerical strain calculations, the results of which are given in Figs. 5 and 6 we use the reliable data for elastic stiffness coefficient taken from Ref. 32 and we also applied Vegard's law for ternary III-nitride alloy crystal lattice parameters and elastic stiffness coefficients. The strains are illustrated for both InGaN and AlGaN layers on GaN templates. Both coordinate systems (P and N systems) were used for the presentation of the results. An important result of our calculations is the appearance of the shear strain component $\varepsilon_{y'z'}$ in the layer in the P-coordinate system. Note that for either equibiaxial mismatch or elastic isotropy, no shear strain would be present in the layer. In Figs. 5 and 6, $\varepsilon_{y'y'}$ component directly demonstrates the dependence of the lattice mismatch on the c-axis inclination in wurtzite semipolar layers. From Fig. 6 we already have an idea why the out-of-plane polarization (but also the total piezoelectric polarization!) may vanish for a particular orientation of the semipolar template. It follows from the strain plots that for $\vartheta \approx 45°$ all normal strain components have the same sign that, together with the opposite sign in piezoelectric coefficients e_{31} and e_{33}, will provide the zero crossover in the polarization dependence on the inclination angle.

To quantitatively characterize the strain-induced polarization, we used the strain results together with Vegard's law for piezoelectric coefficients in the mismatched layer by applying Eq. (18). The results given in Figs. 7 and 8 demonstrate that for both InGaN and AlGaN layers on GaN templates the piezoelectric polarization becomes zero for the nonpolar orientation $\vartheta_N = 90°$ and also for a semipolar orientation $\vartheta_S \approx 45°$ for InGaN layers. Actually, the zero crossover ϑ_S depends on the In or Al content of the ternary alloy layer, but this dependence is very weak for the considered sets of material parameters. With the addition of spontaneous polarization, the angle increases only slightly for InGaN because the values for spontaneous polarization in InN and GaN are very close. For AlGaN mismatched layers, the effect of spontaneous polarization becomes important and an increase of ϑ_S up to $\approx 70°$ was calculated.

We may note here that the application of Vegard's law was primarily confirmed for crystal lattice parameters. For other values such as stiffness coefficients, piezoelectric coefficients, and magnitudes of spontaneous polarizations, direct use of Vegard's law can be considered only as a first approximation. For example, there exists experimental evidence that polarization charge (discontinuity in spontaneous polarization) demonstrates nonlinear behavior in AlGaN/GaN structures depending on Al content.[36,37] Even in this case for small Al concentrations (less than 20%) linear Vegard description gives reasonable model results.[36] The other important issue are the values of spontaneous polarization for III-nitrides. There is considerable scatter in these values in the literature (see, for example, information in Refs. 31 and 35). In our calculations we use as representative example the values of spontaneous polarization in III-nitrides given in Ref. 3.

Analyzing the data from Table I for the inclination angle of low index semipolar crystallographic planes in III-nitrides, we note that $(10\bar{1}\bar{1})$ and $(11\bar{2}\bar{2})$ plane orientations are the closest to the crossover orientation ϑ_S for AlGaN layers when spontaneous polarization was included in the total polarization discontinuity. For InGaN layers, the closest to crossover orientation ϑ_S planes are those with Miller indices $(11\bar{2}\bar{2})$ and $(10\bar{1}\bar{3})$. However, we recall that only $(11\bar{2}\bar{2})$ template has Ga polarity in the outward growth direction. The polarity issue is important for the interpretation of the result. For $[000\bar{1}]$ outward direction the polarization plots should be flipped with respect the ϑ axis, otherwise the polarization dependences should be plotted for $0°-180°$ range.

As mentioned earlier, we have demonstrated $(10\bar{1}\bar{1})$ and $(10\bar{1}\bar{3})$ oriented GaN-based LEDs.[18] The device layers, including the InGaN quantum wells and *n*- and *p*-type layers, were grown by MOCVD on underlying HVPE templates. For both orientations, LEDs demonstrated light emission at 439 nm and exhibited no electroluminescence peak shift with drive currents from 10 to 150 mA, which we attribute to reduced polarization-induced electric fields in the InGaN quantum wells in both semipolar orientations.

In conclusion, strain-induced effects in III-nitride mismatch layers grown on semipolar templates have been addressed. The dependence of piezoelectric polarization on growth orientation and layer composition has been calculated for $In_xGa_{1-x}N$ (or $Al_yGa_{1-y}N$) layers matched with GaN template. It has been shown that piezoelectric polarization becomes zero not only for nonpolar orientation, but also for semipolar templates tilted to $\sim 45°$ from the *c* plane. This crossover orientation was nearly insensitive to spontaneous polarization for InGaN layers but was strongly affected for AlGaN layers.

ACKNOWLEDGMENTS

This work was supported by the JST/ERATO NICP program at UCSB. Additional support was provided through the Solid State Lighting and Display Center at UCSB.

APPENDIX: DETAILS ON STRAIN CALCULATIONS FOR AN ANISOTROPIC MISMATCHED WURTZITE LAYER ON ARBITRARILY ORIENTED SEMIPOLAR WURTZITE TEMPLATE

Instead of using the general form of Hooke's law given by Eq. (11), we write it in a simpler 6×6 Voigt or matrix notation:[10]

$$\sigma_i = C_{ij}\varepsilon_j, \tag{A1}$$

where σ_i and ε_j are the six unique stresses and strains and C_{ij} is the 6×6 matrix form of the elastic stiffness coefficients with the following correspondence among the components in Voigt notation and the usual components of symmetric second-rank stress and strain tensors:

$$\sigma_1 = \sigma_{xx},\ \ \sigma_2 = \sigma_{yy},\ \ \sigma_3 = \sigma_{zz},\ \ \sigma_4 = \sigma_{yz},\ \ \sigma_5 = \sigma_{xz},\ \ \sigma_6 = \sigma_{xy}, \tag{A2}$$

$$\varepsilon_1 = \varepsilon_{xx},\ \ \varepsilon_2 = \varepsilon_{yy},\ \ \varepsilon_3 = \varepsilon_{zz},\ \ \varepsilon_4 = 2\varepsilon_{yz},\ \ \varepsilon_5 = 2\varepsilon_{xz},\ \ \varepsilon_6 = 2\varepsilon_{xy}. \tag{A3}$$

Note the appearance in Eq. (A3) of a coefficient 2 for shear strain components (omitting this factor is the basis for multiple mistakes in the literature).

For wurtzite III-nitrides, the C_{ij} matrix, which has only five independent coefficients, may be written in the *N*-coordinate system with the *z* axis parallel to the *c* direction as

$$C_{ij} = \begin{pmatrix} C_{11} & C_{12} & C_{13} & 0 & 0 & 0 \\ C_{12} & C_{11} & C_{13} & 0 & 0 & 0 \\ C_{13} & C_{13} & C_{33} & 0 & 0 & 0 \\ 0 & 0 & 0 & C_{44} & 0 & 0 \\ 0 & 0 & 0 & 0 & C_{44} & 0 \\ 0 & 0 & 0 & 0 & 0 & \dfrac{C_{11}-C_{12}}{2} \end{pmatrix}. \tag{A4}$$

Substituting Eqs. (A2)–(A4) in (A1) gives the compact form of Hooke's law with components represented in *N*-coordinate system:

$$\begin{aligned} \sigma_{xx} &= C_{11}\varepsilon_{xx} + C_{12}\varepsilon_{yy} + C_{13}\varepsilon_{zz}, \\ \sigma_{yy} &= C_{12}\varepsilon_{xx} + C_{11}\varepsilon_{yy} + C_{13}\varepsilon_{zz}, \\ \sigma_{zz} &= C_{13}\varepsilon_{xx} + C_{13}\varepsilon_{yy} + C_{33}\varepsilon_{zz}, \\ \sigma_{yz} &= 2C_{44}\varepsilon_{yz}, \\ \sigma_{xz} &= 2C_{44}\varepsilon_{xz}, \\ \sigma_{xy} &= (C_{11}-C_{12})\varepsilon_{xy}. \end{aligned} \tag{A5}$$

Then we transform the stresses to the *P*-coordinate system by applying the rotation (via a proper transformation of the second-rank stress tensor) about the *x* axis by the angle ϑ:

$$\begin{aligned} \sigma_{x'x'} &= \sigma_{xx}, \\ \sigma_{y'y'} &= \sigma_{yy}\cos^2\vartheta + \sigma_{zz}\sin^2\vartheta - \sigma_{yz}\sin 2\vartheta, \\ \sigma_{z'z'} &= \sigma_{yy}\sin^2\vartheta + \sigma_{zz}\cos^2\vartheta + \sigma_{yz}\sin 2\vartheta, \\ \sigma_{y'z'} &= \frac{\sigma_{yy}-\sigma_{zz}}{2}\sin 2\vartheta + \sigma_{yz}\cos 2\vartheta, \\ \sigma_{x'z'} &= \sigma_{xz}\cos\vartheta + \sigma_{xy}\sin\vartheta, \\ \sigma_{x'y'} &= \sigma_{xy}\cos\vartheta - \sigma_{xz}\sin\vartheta. \end{aligned} \tag{A6}$$

Note that we use only one angle in the tensor transformation between the *N*- and *P*-coordinate systems (instead of two angles in the case of a general rotation matrix) because of the property of isotropy of the basal plane of the wurtzite crystal structure. Substituting Eq. (A5) in Eq. (A6), we express the strains ε_{ij} via the strains $\varepsilon_{k'm'}$ [similar to Eqs. (13) in the main text] that eventually give us the system of six equations:

$$\sigma_{x'x'} = C_{11}\varepsilon_{x'x'} + (C_{12}\cos^2\vartheta + C_{13}\sin^2\vartheta)\varepsilon_{y'y'} + (C_{12}\sin^2\vartheta + C_{13}\cos^2\vartheta)\varepsilon_{z'z'} + (C_{12} - C_{13})\sin 2\vartheta\varepsilon_{y'z'},$$

$$\sigma_{y'y'} = (C_{12}\cos^2\vartheta + C_{13}\sin^2\vartheta)\varepsilon_{x'x'} + \left(C_{11}\cos^4\vartheta + \frac{C_{13}+2C_{44}}{2}\sin^2 2\vartheta + C_{33}\sin^4\vartheta\right)\varepsilon_{y'y'} + \left[\left(\frac{C_{11}+C_{33}}{4} - C_{44}\right)\sin^2 2\vartheta + C_{13}(\sin^4\vartheta + \cos^4\vartheta)\right]\varepsilon_{z'z'} + \sin 2\vartheta[(C_{11} - C_{13})\cos^2\vartheta + (C_{13} - C_{33})\sin^2\vartheta - 2C_{44}\cos 2\vartheta]\varepsilon_{y'z'},$$

$$\sigma_{z'z'} = (C_{12}\sin^2\vartheta + C_{13}\cos^2\vartheta)\varepsilon_{x'x'} + \left[\left(\frac{C_{11}+C_{33}}{4} - C_{44}\right)\sin^2 2\vartheta + C_{13}(\sin^4\vartheta + \cos^4\vartheta)\right]\varepsilon_{y'y'} + \left[C_{33}\cos^4\vartheta + \left(\frac{C_{13}}{2} + C_{44}\right)\sin^2 2\vartheta + C_{11}\sin^4\vartheta\right]\varepsilon_{z'z'} + [(C_{11} - C_{13})\sin^2\vartheta + (C_{13} - C_{33})\cos^2\vartheta + 2C_{44}\cos 2\vartheta]\sin 2\vartheta\varepsilon_{y'z'},$$

$$\sigma_{y'z'} = \frac{C_{12} - C_{13}}{2}\sin 2\vartheta\varepsilon_{x'x'} + \left(\frac{C_{11} - C_{13}}{2}\cos^2\vartheta + \frac{C_{13} - C_{33}}{2}\sin^2\vartheta - C_{44}\cos 2\vartheta\right)\sin 2\vartheta\varepsilon_{y'y'} + \left(\frac{C_{11} - C_{13}}{2}\sin^2\vartheta + \frac{C_{13} - C_{33}}{2}\cos^2\vartheta + C_{44}\cos 2\vartheta\right)\sin 2\vartheta\varepsilon_{z'z'} + \left[\left(\frac{C_{11}+C_{33}}{2} - C_{13}\right)\times\sin^2 2\vartheta + C_{44}\cos^2 2\vartheta\right]\varepsilon_{y'z'},$$

$$\sigma_{x'z'} = 2C_{44}(\cos\vartheta + \sin\vartheta)\cos\vartheta\varepsilon_{x'z'} - 2C_{44}(\cos\vartheta + \sin\vartheta)\sin\vartheta\varepsilon_{x'y'},$$

$$\sigma_{x'y'} = [(C_{11} - C_{12})\cos^2\vartheta + 2C_{44}\sin^2\vartheta]\varepsilon_{x'y'} + (C_{11} - C_{12} - 2C_{44})\sin\vartheta\cos\vartheta\varepsilon_{x'z'}. \quad \text{(A7)}$$

Applying the conditions of Eqs. (9) and (10) to the above system, one easily obtains

$$\varepsilon_{x'z'} = 0 \quad \text{(A8)}$$

and

$$\sigma_{x'y'} = 0. \quad \text{(A9)}$$

We may note that the third and fourth equations in Eqs. (A7) constitute the separate linear system for two unknown strains $\varepsilon_{z'z'}$ and $\varepsilon_{y'z'}$ in the P coordinates. The analytical solutions for these strains are given in the main part as the third and fourth lines in Eqs. (12).

[1] S. Nakamura, G. Fasol, and S. J. Pearton, *The Blue Laser Diode* (Springer, New York, 2000).
[2] L. F. Eastman and U. K. Mishra, IEEE Spectrum **39**, 28 (2002).
[3] F. Bernardini, V. Fiorentini, and D. Vanderbilt, Phys. Rev. B **56** R10024 (1997).
[4] F. Bernardini and V. Fiorentini, Phys. Status Solidi B **216**, 391 (1999).
[5] T. Takeuchi *et al.*, Appl. Phys. Lett. **73**, 1691 (1998).
[6] I. J. Seo, H. Kollmer, J. Off, A. Sohmer, F. Scholz, and A. Hangleiter, Phys. Rev. B **57**, R9435 (1998).
[7] R. Langer, J. Simon, V. Oritz, N. T. Pelekanos, A. Barski, R. Andre, and M. Godlewski, Appl. Phys. Lett. **74**, 3827 (1999).
[8] P. Lefebvre, J. Allegre, B. Gil, H. Mathieu, N. Grandjean, M. Leroux, J. Massies, and P. Bigenwald, Phys. Rev. B **59**, 15363 (1999).
[9] P. Lefebvre *et al.*, Appl. Phys. Lett. **78**, 1252 (2001).
[10] J. F. Nye, *Physical Properties of Crystals* (Oxford University Press, New York, 1985).
[11] G. D. O'Clock, Jr. and M. T. Duffy, Appl. Phys. Lett. **23**, 55 (1973).
[12] S. Muensit, E. M. Goldys, and I. L. Guy, Appl. Phys. Lett. **75**, 3965 (1999).
[13] R. D. King-Smith and D. Vanderbilt, Phys. Rev. B **47**, 1651 (1993).
[14] K. Shimada, T. Sota, and K. Suzuki, J. Appl. Phys. **84**, 4951 (1998).
[15] P. Waltereit, O. Brandt, A. Trampert, H. T. Grahn, J. Menniger, M. Ramsteiner, M. Reiche, and K. H. Ploog, Nature (London) **406**, 865 (2000).
[16] M. D. Craven, S. H. Lim, F. Wu, J. S. Speck, and S. P. DenBaars Appl. Phys. Lett. **81**, 469 (2002).
[17] T. J. Baker, B. A. Haskell, F. Wu, P. T. Fini, J. S. Speck, and S. Nakamura, Jpn. J. Appl. Phys., Part 2 **44**, L920 (2005).
[18] A. Chakraborty *et al.*, Jpn. J. Appl. Phys., Part 2 **44**, L945 (2005).
[19] U. M. E. Christmas, A. D. Andreev, and D. A. Faux, J. Appl. Phys. **98**, 073522 (2005).
[20] J. W. Matthews, in *Dislocations in Solids*, edited by F. R. N. Nabarro (North-Holland, Amsterdam, 1979), Vol. 2, 461.
[21] J. A. Floro, D. M. Follstaedt, P. Provencio, S. J. Hearne, and S. R. Lee, J. Appl. Phys. **96**, 7087 (2004).
[22] P. Cantu, F. Wu, P. Waltereit, S. Keller, A. E. Romanov, S. P. DenBaars, and J. S. Speck, J. Appl. Phys. **97**, 103534 (2005).
[23] A. Bykhovski, B. Gelmont, and M. Shur, Appl. Phys. Lett. **63**, 2243 (1993).
[24] S.-H. Park and S.-L. Chang, Phys. Rev. B **59**, 4725 (1999).
[25] T. Takeuchi, H. Amano, and I. Akasaki, Jpn. J. Appl. Phys., Part 1 **39**, 413 (2000).
[26] S.-H. Park, Jpn. J. Appl. Phys., Part 1 **42**, 5052 (2003).
[27] D. L. Smith, Solid State Commun. **57**, 919 (1986).
[28] D. L. Smith and C. Mailhiot, J. Appl. Phys. **63**, 2717 (1988).
[29] D. Sun and E. Towe, Jpn. J. Appl. Phys., Part 1 **33**, 702 (1994).
[30] T. Baker, B. Haskell, F. Wu, J. Speck, and S. Nakamura, Jpn. J. Appl. Phys., Part 2 **45**, L154 (2006).
[31] I. Vurgaftman and J. Meyer, J. Appl. Phys. **94**, 3675 (2003).
[32] A. F. Wright, J. Appl. Phys. **82**, 2833 (1997).
[33] J. G. Gualtieri, IEEE Trans. Ultrason. Ferroelectr. Freq. Control **4**, 53 (1994).
[34] A. E. Romanov, P. Waltereit, and J. S. Speck, J. Appl. Phys. **97**, 043708 (2005).
[35] O. Ambacher *et al.*, Phys. Status Solidi C **0**, 4340 (2003).
[36] E. J. Miller, E. T. Yu, C. Poblenz, C. Elsass, and J. S. Speck, Appl. Phys. Lett. **80**, 3551 (2002).
[37] A. T. Winzer, R. Goldhahn, G. Gobsch, A. Link, M. Eickhoff, U. Rossow, and A. Hangleiter, Appl. Phys. Lett. **86**, 181912 (2005).